Molecular evidence for an activator–inhibitor mechanism in development of embryonic feather branching

Matthew P. Harris*†‡, Scott Williamson§, John F. Fallon*, Hans Meinhardt¶, and Richard O. Prum‡∥

*Department of Anatomy, 1300 Bardeen, University of Wisconsin, Madison, WI 53706; §Department of Biological Statistics and Computational Biology, 101 Biotech, Cornell University, Ithaca, NY 14853; ¶Max Plank Institute für Entwicklungsbiologie, Abt. Evolutionsbiologie, Spemanstrasse 35, 72072 Tübingen, Germany; and ∥Department of Ecology and Evolutionary Biology, and Peabody Museum of Natural History, Yale University, P. O. Box 208105, New Haven, CT 06520

The developmental basis of morphological complexity remains a central question in developmental and evolutionary biology. Feathers provide a unique system to analyze the development of complex morphological novelties. Here, we describe the interactions between Sonic hedgehog (Shh) and bone morphogenetic protein 2 (Bmp2) signaling during feather barb ridge morphogenesis. We demonstrate that activator–inhibitor models of Shh and Bmp2 signaling in the tubular feather epithelium are sufficient to explain the initial formation of a meristic pattern of barb ridges and the observed variation in barb morphogenesis in chick natal down feathers. Empirical tests support the assumptions of the model that, within the feather ectoderm, Shh (activator) up-regulates its own transcription and that of Bmp2 (inhibitor), whereas Bmp2 signaling down-regulates Shh expression. More complex models incorporating a second activator and dorsal/ventral polarized modification of activator signaling can produce all of the barb morphogenesis patterns observed during the growth of more complex branched pennaceous feathers: new barb ridge formation, helical growth, and barb ridge fusion. An integrated model of feather morphogenesis and evolution suggests that plumulaceous feather structure evolved by the establishment of activator–inhibitor interactions between Shh and Bmp2 signaling in the basal epithelium of the feather germ. Subsequently, pennaceous feather structure evolved through the integration of barb ridge morphogenesis with a second, local inhibitor and a dorsal/ventral signal gradient within the feather. The model is congruent with paleontological evidence that plumulaceous feathers are primitive to pennaceous feathers.

evolution | Shh | Bmp2 | branching morphogenesis | pattern formation

Feathers are complex morphological structures that encompass many morphological novelties (1–3). Through natural and sexual selection, evolution of the developmental specification of feathers has produced a diversity of morphologies that function in a variety of ways in the lives of birds (4). The most basic structural component of the feather is the barb (1–3). Variation in barb number and branching pattern contributes to the diversity in feather form and function (3, 5). Here, we investigate the molecular developmental basis of the formation of barb number and barb branching structure.

The formation of barbs within the undifferentiated conical epithelium of the embryonic feather bud requires the function of several developmental signaling systems, including the coordinated signaling of Sonic hedgehog (Shh) and bone morphogenetic protein 2 (Bmp2) (6). Our previous work suggests that aspects of the pattern and polarity within feather epithelia develops by the concerted action of Shh and Bmp2 signaling within the epithelia (6).

To investigate the dynamics of molecular signaling during feather barb morphogenesis, we have applied activator–inhibitor models to the developing feather germ. Activator–inhibitor models have proven to be a powerful heuristic tool in the investigation of developmental patterning in biological systems (7–10). In their simplest form, these models hypothesize a locally self-enhancing activator that stimulates the production of a long-range antagonistic inhibitor that also reduces the production of the activator (7, 11). If morphogenesis is linked to a critical threshold in activator concentration, the result can be a stable, spatial pattern in morphology. The interactions between Shh and Bmp2 during feather barb morphogenesis makes them good molecular candidates for such signaling dynamics.

Here, we show that Shh and Bmp2 signaling can explain the formation of, and variation in, the pattern of barb ridges in a plumulaceous feather by an activator–inhibitor mechanism. More advanced models predict that the development of more complex pennaceous feathers, including helical growth of barb ridge and rachis formation, requires an additional short-range but long-acting inhibitory signal and a polarized dorsal/ventral (D/V) signal gradient. These findings present direct, molecular evidence of an activator–inhibitor mechanism in meristic (i.e., iterative, modular) pattern formation during animal development. Further, the molecular details of feather barb morphogenesis support previously uncharacterized conclusions about the evolution of downy and pennaceous feathers.

Background

The first feathers form from a thickening of the embryonic epidermis, the placode (Fig. 1 A and B, lower), that elongates into a short conical outgrowth called the feather bud (Fig. 1 A and B, upper). At this early stage, the simple conical epithelium of the feather bud is regionally polarized (6, 12, 13). Subsequently, longitudinal invaginations of the basal epithelium of the feather bud, called the marginal plate, form the edges of the developing barb ridges (Fig. 1C). Each barb ridge grows in length by recruiting new cells, which proliferate at the growing base of the feather germ, to join the base of that barb ridge (3, 14, 15). The variations in the initial number of barb ridges will directly affect the shape, and consequent function, of the feather (5).

Simple plumulaceous, or downy, feathers do not have a prominent rachis; the barbs are fused in a tuft at the base to the tubular calamus (Fig. 1E). In contrast, pennaceous feathers have a planar vane and a shaft, called the rachis (Fig. 1H). The rachis and planar vane of a pennaceous feather are produced by helical growth of barb ridges around the tubular feather germ (1–3). Barb ridges grow helically by recruiting new cells to become part of that barb ridge
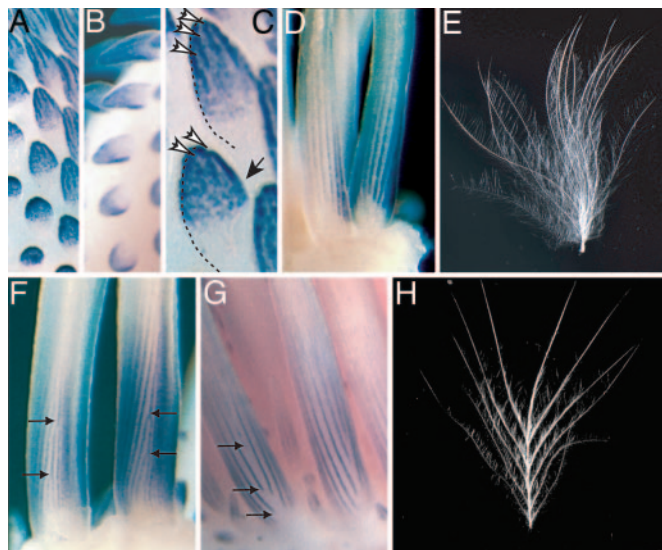
Fig. 1. Expression dynamics of Shh and Bmp2 in developing embryonic feather buds of plumulaceous and pennaceous feathers. Shh (*A*) and Bmp2 (*B*) are expressed in overlapping regions during the development of the feather bud. (*C*) Shh expression is diffuse in early buds but becomes refined into longitudinal domains, or stripes, in the marginal plate epithelium at the edge of the forming barbs (white arrows) from the initial diffuse expression (black arrow). (*D*) In plumulaceous down feathers of the chick, the longitudinal Shh expression domains run parallel as the feather grows in length from the bottom. (*E*) The simple, tufted, plumulaceous, natal down feather of a chick lacks a rachis. (*F* and *G*) Pennaceous feather germs in embryonic ducks exhibit helical growth of barb ridges from the ventral (*F*) to dorsal (*G*) surfaces. Ventral bifurcation of Shh stripes (*F,* arrows) leads to the addition of new barb ridges, whereas dorsal extinction of Shh stripes (*G,* arrows) produces fusion of barb ridges to create the rachis ridge and branched feather form. (*H*) A pennaceous natal duck feather has a prominent rachis and planar form.

from successively more dorsal radial positions within the tubular feather germ. Initially, barb ridges fuse on the dorsal side of the feather germ to form the rachis ridge, and subsequent barb ridges fuse to the rachis.

In forming feather buds, Shh and Bmp2 are necessary for barb ridge formation and differentiation (6). Shh is expressed broadly in the entire marginal plate epithelium; Bmp2 is expressed exclusively at the peripheral bend of the marginal plate epithelium where it overlaps with Shh expression (6). Thus, Shh and Bmp2 form linear expression domains, or stripes, that indicate the edges of the forming barb ridges (Fig. 1*D*). To visualize the developing feather from the stripes of Shh and Bmp2 prepattern, it is critical to remember that the tissue between the stripes will form the feather barbs (Fig. 1 *D–H*). In weakly polarized embryonic feathers of chick, the longitudinal stripes for Shh and Bmp2 expression match the simple, tufted morphology of chick natal down (Fig. 1 *D* and *E*). Variations in Shh/Bmp2 expression during barb ridge morphogenesis also match phenotypic variation in barb number and branching structure (6). In plumulaceous embryonic feather germs of chick, we found four variants in the linear Shh/Bmp2 expression domains: bifurcation, extinction (or cessation), fusion, and initiation (6). Each of these stripe variants is associated with a distinct form of branched barb morphogenesis: new barb formation, barb fusion, a free or unattached barb, and a pair of barbs fused at the tip, respectively (6). The pennaceous natal feathers of a duck embryo develop through coordination and polarized utilization of two of the four stripe variants observed in plumulaceous chick down.

On the ventral midline of the pennaceous germ where new barb ridges originate, Shh and Bmp2 stripes bifurcate (arrows, Fig. 1*F*). After growing helically around the tubular feather germ, the expression domains extinguish as they approach the dorsal midline

(Fig. 1*G*). The result is the creation of new barb ridges on the ventral side and barb ridge fusion and rachis creation on the dorsal side. Therefore, coordinated utilization of variability seen during development of the barbs of a plumulaceous down feather (e.g., chick) is the basis of the formation of a complex branching pattern of the pennaceous feather (e.g., duck) (Fig. 1 *E* and *H*; ref. 6). Ultimately, the tubular feather germ emerges from the superficial sheath and unfurls to form the planar vane (Fig. 1*H*) (1, 3, 5, 6).

A developmental model of the evolution of feathers has predicted that feathers evolved through a series of developmental novelties from simple tubes, to a downy tuft of barbs, and, ultimately, to a pennaceous structure with a planar vane (1). Independent evidence in support of the prediction that plumulaceous feathers are primitive to pennaceous feather has come from fossil feathers of nonavian theropod dinosaurs and from the pattern of evolutionary cooption of the Shh-Bmp2 molecular module in feather development (6, 16).

Methods

Mathematical Models. The activator–inhibitor models used were developed in previous studies (8, 17, 18). Barb morphogenesis in the tubular feather germ was modeled as a temporal series of ring-shaped spatial fields of a given circumference. Growth was simulated by the addition of a new ring at the base of the tube. In some simulations (Fig. 2*G*), the circumference of the field grew in size through the addition of new cells at random positions within the ring. The ability of the cells to perform the autocatalytic reaction, *s*, was modulated by maximum 1% random fluctuations. The simplest simulations used a two-component activator–inhibitor model

$$\frac{\partial a}{\partial t} = \frac{s(a^2 + b_a)}{(1 + s_a a^2)(b + s_c c)} - r_a a + D_a \frac{\partial^2 a}{\partial x^2} \qquad [1]$$

$$\frac{\partial b}{\partial t} = r_a a^2 + b_b - r_b b + D_b \frac{\partial_2 b}{\partial x^2,} \qquad [2]$$

where $a(x, t)$ and $b(x, t)$ represent the activator and inhibitor concentrations, respectively (8). s_a causes saturation of the activator autocatalysis at high activator concentrations. ($s_c c$ is only relevant for the three-component system described below). b_a and b_b are the activator-independent, background production rates of the activator and inhibitor; b_a is responsible for insertion of new activator peaks into gaps between existing peaks, and b_b inhibits the creation of new peaks. r_a and r_b are the decay rates, and D_a and D_b are the diffusion rates, respectively.

Helical growth was simulated by the addition of a second inhibitor c(x,t) that is local and long acting

$$\frac{\partial c}{\partial t} = b_c a^2 - r_c c. \qquad [3]$$

r_c is the decay rate of the second inhibitor. In this version, both inhibitors are assumed to act in an additive way (8, 18). Additional simulations were performed in which there was also a D/V polarization of inhibitor activity. A dorsal increase and ventral decrease in the level basic inhibitor production (b_b) was hypothesized. More details can be found in refs. 7, 8, 11, 17, 19, and 20.

Specimen Collection and Preparation. Eggs of the Babcock strain of White Leghorn chickens (*Gallus gallus*; University of Wisconsin, Madison), scaleless (University of Connecticut, Storrs, CT), and SPAFAS (Charles River Laboratories) lines were incubated at 39°C until needed. Khaki Campbell duck eggs (*Anas platyrhynchus*) from Metzer Farms (Gonzalez, CA) were incubated with added humidity. Embryos were fixed overnight in 4% paraformaldehyde/PBS, dehydrated in a methanol series, and stored at −20°C until used.
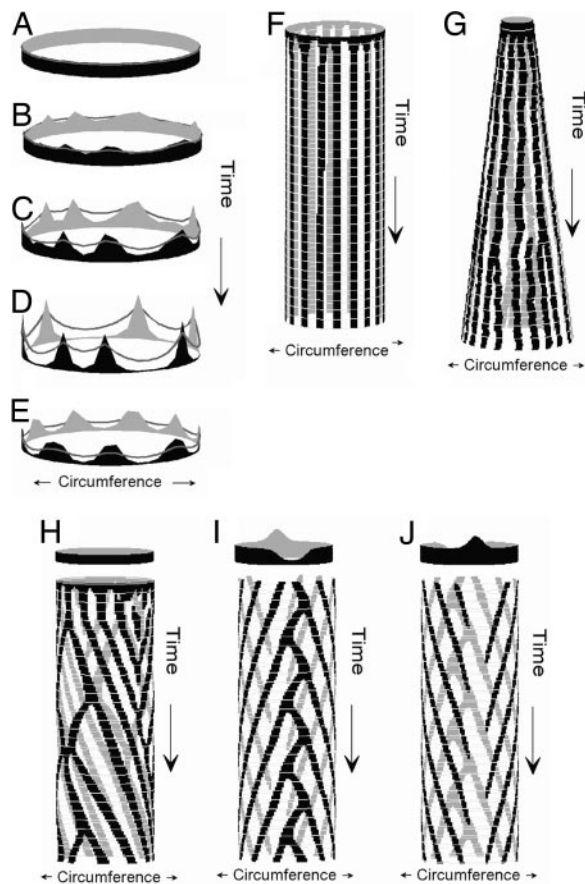
Fig. 2. Activator–inhibitor models are sufficient to describe the establishment of barb patterning within embryonic feather buds. (*A–D*) A time series of rings that show the concentration of activator (solid areas) and inhibitor (lines) in a two-component model (Eqs. **1** and **2**) producing a stable equilibrium of activator and inhibitor concentrations (*D*). (*E*) Stable activator and inhibitor concentrations for a ring in a two-component model with activator saturation. (*F*) Simulation of barb patterning in a tubular feather germ by a two-component model showing the establishment of a stable number and position of stripes of peak activator concentration from random initial concentrations. (*G*) Simulation of barb patterning in a feather germ with a growing circumference by using a two-component model with local activator saturation. These conditions create opportunities for initiation of new activator peaks and bifurcation of existing peaks. (*H*) Simulation of barb patterning in a tubular feather germ by using a three-component model (Eqs. **1–3**) and uniform background activator production (circle at top). The stripes of activator concentration grow helically like traveling waves because of an additional, local inhibitor. Positional instability creates opportunities for activator stripe bifurcation, fusion, and cessation, but they are not localized to any particular position in the tube. (*I* and *J*) Ventral (*I*) and dorsal (*J*) views of a simulation of barb patterning in a tubular feather germ using a three-component model with ventral decrease and dorsal increase in the background level of activator production (b_b in Eq. **1**, circles at top). Lowered inhibition of activator autocatalysis causes activator saturation level and leads to stripe branching on the ventral side. The elevated levels of inhibition lead to an extinction of activation peaks as they reach the dorsal side.

Retroviral Infection. RCAS viruses were produced by the following procedures in ref. 21. All retroviral expression experiments were performed in SPAFAS. RCAS infections were made into the amnion of s26 embryos and harvested at embryonic day 9–10 for whole-mount analyses. RCAS containing constitutively active BMPR1, Shh, and RCAN control have been described in refs. 22 and 23.

Whole Mount *in Situ* and Immunohistochemistry. Whole-mount *in situ* labeling was performed as described in ref. 24 with the addition of

10% polyvinyl alcohol to the color reaction after fixation in paraformaldehyde and subsequent clearing in methanol. For single-color analysis, the signal was detected by using alkaline phosphatase-conjugated antibodies and nitroblue tetrazolium (NBT)/5-bromo-4-chloro-3-indolyl phosphate (BCIP) as a substrate. To detect RCAS expression, the antibody AMV-3c2 (Iowa Developmental Studies Hybridoma Bank) was used either prior to or subsequent to detection of Digoxygenin-labeled transcripts. For double-labeled experiments, 2-[4-iodophenyl]-3-[4-nitrophenyl]-5-phenyl-tetrazolium chloride (INT)/BCIP was detected first, and followed by stripping the antibody in glycine HCl (pH 2), further antibody detection of the second antigen, and detection by NBT/BCIP. Endogenous expression labeled by INT/BCIP often was decreased during the second detection; however, ectopic expression was maintained. Probes for analysis of Shh and Bmp2 expression were kindly provided by Cliff Tabin (Harvard Medical School, Boston).

Histochemistry. Feather tissue was embedded in paraffin by using xylene as antimedium, sectioned at 5- to 7-μm thickness, and stained with hematoxylin/eosin per standard protocols. Sections of tissue after whole-mount *in situ* analysis were accomplished by using isopropanol as an antimedium for paraffin embedment. INT/BCIP precipitate, however, was soluble in all antimedia tested and could not be sectioned by using paraffin.

Results

Models of Feather Branching Pattern. The simplest, two-component models simulate the origin of an integer number of activator peaks within a circular field of cells from a random distribution of initial activator and inhibitor concentrations (Fig. 2 *A–D*). As the ring grows into a tubular feather germ by cell division at its base, the activator peaks will produce longitudinal stripes that are highly stable in radial position (Fig. 2*F*). For a given set of parameter values, the number of stable activator peaks, or stripes, depends on the size of the morphogenic field (7, 8).

An additional saturation parameter limits the local production of the activator and leads to a broadening of activator peaks (Fig. 2*E*). The center of an activator peak can then become deactivated because of the lateral inhibition from the cell on its flanks. In simulations in which the morphogenic field grows in circumference as well as length, saturation produces bifurcation in the longitudinal stripes of activator concentration and the initiation of new activator peaks (Fig. 2*G*).

A three-component model, including an additional short-range (i.e., cell autonomous), long-duration inhibitor, can simulate all variants in activator stripe propagation dynamics, including helical growth, bifurcation, extinction, fusion, and initiation (Fig. 2*H*). The second inhibitor creates "traveling waves" of peak activator concentration by locally quenching activator production and causing helical propagation of activator peaks (8). However, the direction of helical growth and the radial position of the stripe instabilities are randomly determined and not predictably polarized (Fig. 2*H*).

With a polarized D/V signal gradient, a three-component system can simulate the origin of a discrete number of barb ridges, bifurcation of activator stripes on the ventral side, helical growth of barb ridges toward the dorsal side, and extinction of activator stripes as they approach the dorsal midline (Fig. 2 *I* and *J*). Specifically, ventrally reduced inhibitor production causes activator saturation and the initiation of new waves by activator peak bifurcation on the ventral side, whereas dorsally increased inhibitor production causes the extinction of traveling waves of activator concentration on the dorsal side.

Tests of Two-Component Model Assumptions. The fundamental assumptions of the two-component model are as follows: (*i*) the inhibitor down-regulates activator function, (*ii*) the activator up-regulates its own expression, and (*iii*) the activator increases the
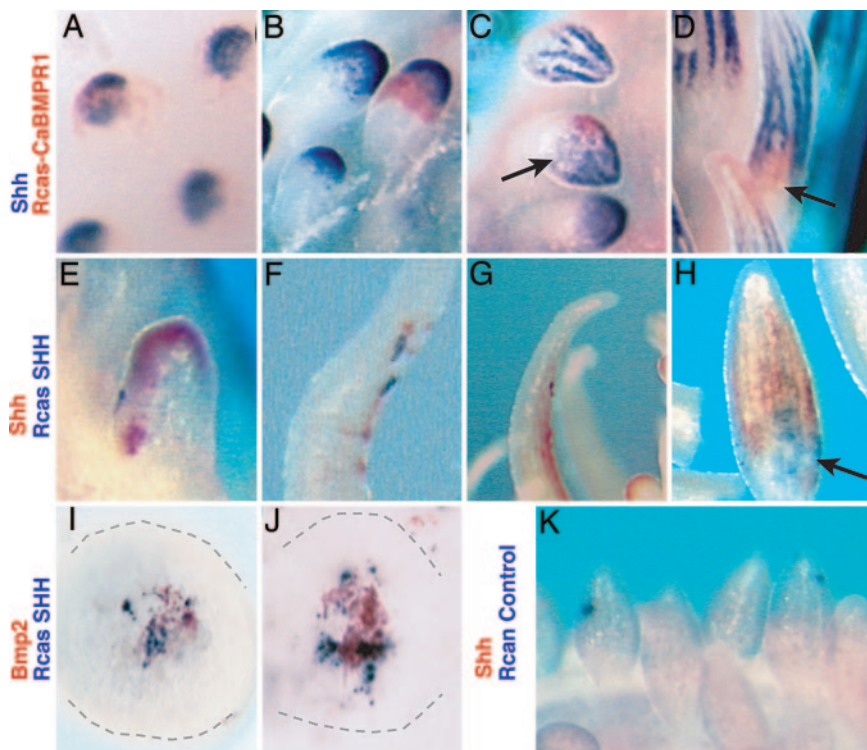
Fig. 3. Effects of forced expression of molecular mediators of Shh and Bmp signaling in feather germs by using localized RCAS infections of the ectoderm during outgrowth and formation of barb ridge pattern. (*A–D*) Foci of virus expressing a constitutively active BMP receptor 1 (red, caBMPR1) showed a cell autonomous down-regulation of endogenous Shh expression (blue) in placode (*A*) and early bud stages (*B*) and during barb specification (*C* and *D*). Effect of the virus expression on Shh expression is also seen far from the site of infection (*C*). (*E–H*) Virus expressing Shh (blue, RCAS-SHH) caused up-regulation of endogenous Shh expression (red) in early feather buds (*E*) and later feather filaments (*F-H*). This effect was seen far from the site of ectopic expression, indicating the long-distance signaling capacity of Shh in the feather epithelium. (*I* and *J*) Infection of RCAS-SHH up-regulated endogenous Bmp2 expression (red) in small feather buds (gray outline). Bmp2 expression was detected only near infection sites. (*K*) Effect of control RCAS virus (blue) on endogenous Shh expression (red). Normal Shh and Bmp2 expression in E-H is present, but the red INT/NBT precipitate is not as sensitive or stable as BCIP/NBT and is diminished in the two-color procedure.

activity of the inhibitor. We have previously shown that integrated Shh and Bmp2 signaling is necessary for barb ridge morphogenesis and that Bmp2 signaling suppresses Shh expression within the marginal plate epithelium of developing feather germs (6). These data support the inhibitory role of Bmp2 signaling on Shh expression during formation of barb ridges; however, our previous studies used ectopic protein treatments that affect both the mesenchyme and epithelia and have effects over the entire feather bud (6). Here, we directly test the interactions between Shh and Bmp2 signaling in the epithelium of the developing feather during barb ridges specification by using viruses that drive Bmp or Shh signaling exclusively in local patches of cells in the epidermis. Injection of RCAS viruses into the amniotic fluid of developing chick limits expression to the ectoderm (25). By injecting virus into the amniotic fluid of s26 embryos (embryonic day 5–6), we were able to localize expression to distinct foci in forming feathers of embryonic day 10 chicks without affecting prior development of the feather placode or growth of the feather bud.

Inhibitor suppression of activator function. To test the role of Bmp signaling in regulating Shh expression, we overexpressed a constitutively active BmpR1 receptor (caBMPR1) (22) in the feather bud epithelium (Fig. 3 *A–D*). These infections simulate the persistent stimulation of Bmp signaling locally in the infected cells. Regional infections of feather buds were detected by using a specific antibody to a viral epitope (red) at various stages of developing feather buds, including just before and during barb specification (Fig. 3 *A–D*). Overexpression of caBMPR1 led to regional and specific down-regulation of Shh expression (blue; 81%, $n = 22$). The effect in early buds seems confined to the region expressing the virus as sharp boundaries are formed between virus infected and endogenous Shh

expression (see Fig. 3 *A*, *B*, and *D*). However, locally increased Bmp signaling disrupted the organization of the longitudinal stripes of Shh expression away from the infection source in two feather buds (Fig. 3*C*, arrow). Localized activation of Bmp signaling by viral infection disrupted barb specification, delineated by Shh expression (Fig. 3*D*). These data indicate that Bmp signaling in the feather epithelium exhibits negative regulation of Shh expression during barb specification.

Activator autocatalysis. We used a similar experimental design to test whether Shh could up-regulate its own expression during barb formation in feather development. Infections of virus driving Shh expression in the feather epithelium (RCAS-Shh; blue) led to the up-regulation of endogenous Shh message (red) within the feather epidermis (Fig. 3 *E–H*; 39%, $n = 64$). Up-regulation of Shh occurred at considerable distance away from the infection source. [Infections with control virus (RCAN) showed no change in pattern or levels of Shh expression (Fig. 3*K*; $n = 16$].

Activator regulation of inhibitor. Regional overexpression of Shh in the feather epidermis (RCAS-Shh; blue) led to detectable up-regulation of Bmp2 expression around the infection sites (Fig. 3 *I* and *J*; 11.8%, $n = 228$) when compared with control virus infections (4.5%; $n = 66$, X^2 $P > 0.001$, data not shown). All observed up-regulation of Bmp2 expression by Shh were found in small feather buds during the process of outgrowth. This finding supports the basic assumption of the model that the activator up-regulates the inhibitor. However, the limitation of the localized effects of Shh expression and lack of detection in more mature feather buds does not support additional conclusions. It is unclear whether the limited signaling range is a product of the assay detection limits (see *Methods*) or a property of the system.

Signal diffusion. Shh and Bmp2 are extracellular proteins that diffuse in the extracellular environment (26–28). We show that Shh expressed within the feather epithelium can elicit endogenous Shh expression at distances that range over several cell lengths (Fig. 3 *D–G*). In addition, activation of Bmp signaling in specific cells during barb ridge specification shows noncell autonomous effects on Shh expression in other cells (Fig. 3*C*). These data indicate that the effect of Shh and Bmp signaling can affect signaling away from the infection source and supports the realism of the diffusion parameters of the models. This effect could be caused by physical diffusion or by signaling among epithelial cells through other signaling cascades. The diffusion parameter in the model describes the net decrease in effect of molecular signals over distance and can be satisfied by either mechanism.

Congruence Between Models and Feather Development. Shh and Bmp2 are initially coexpressed in the distal epidermis of the feather bud (Fig. 1 *A* and *B*). This initially diffuse expression becomes refined into longitudinal stripes of expression that demarcate the marginal plate tissue between the forming barb ridges. The dynamics of Shh/Bmp2 expression patterns observed in feather buds conforms closely to the establishment of stripes of activator concentration simulated by the simple two-component model (compare Figs. 1 *A–D* and 2 *A–D* and *F*). Furthermore, saturation of activator production in a two-component model reproduces some of the variants in longitudinal stripe propagation observed in unpolarized plumulaceous feather germs of chick, such as stripe bifurcation and new stripe initiation (Fig. 2*G*).

The two-component model further predicts that the number of barbs within a feather will depend on the size of the morphogenic field (i.e., circumference of feather epithelium). Accordingly, barb morphogenesis should be the result of a space-filling mechanism, not rigidly fixed to a specific number (Fig. 2*C*). To test this prediction, we compared the number of barb ridges in embryonic duck feather germs of different size classes and in feather germs of a mutant chicken breed with enlarged feather size (see Fig. 4, which is published as supporting information on the PNAS web site). Our findings indicate that the barb number is proportional to the circumference of the feather germ in all feather types examined (Fig. 4). A plot of feather germ circumference and barb ridge number for a diverse sample of embryonic chick and duck feathers documents a strikingly linear relationship (Fig. 4). Apparently, a common mechanism of barb ridge pattern formation is shared by a broad diversity of feathers. Barb ridge morphogenesis in embryonic feathers is congruent with the space-filling prediction of the activator–inhibitor model.

A three-component model with an additional short-range, long-duration inhibitor can reproduce all of the dynamics observed in embryonic plumulaceous feather germs, including helical growth, stripe bifurcation, extinction, fusion, and initiation (Fig. 2*G*). Furthermore, stripe instability in the models occurs at random positions around the feather germ, as observed in plumulaceous chick down, which lack a strongly polarized morphology (6). However, in pennaceous feathers, stripe bifurcation and extinction are restricted to the ventral and dorsal regions, respectively (6) (Fig. 1 *F* and *G*).

A three-component model with an additional D/V polarity in the production of the background inhibitor accurately simulates the entire suite dynamics exhibited in pennaceous feather growth, including meristic patterning of barb ridges, ventral stripe bifurcation resulting in new barb ridge creation, helical growth of activator peaks toward the dorsal side, and stripe extinction and barb ridge fusion on the dorsal side forming the rachis (Figs. 1 *F* and *G* and 2 *I* and *J*).

Discussion

Our data provide an empirically tested example of an activator–inhibitor mechanism during the formation of complex, meristic patterns during development. Activator–inhibitor models have been used to predict developmental patterning of many different animals. These models accurately predict the pattern and variance seen in pigment stripes in growing butterflyfish (9) and zebrafish (29). The genetic mechanisms of activator–inhibitor models have been suggested by the correspondence between the models and the morphologies of a graded allele series of the *leopard* gene in zebrafish (29). Further, an activator–inhibitor model of mammal tooth cusp development accurately predicts changes in gene expression patterns during development of different tooth morphologies; these models are supported by functional analysis of the some of the genes involved (10). The molecular basis underlying these patterning processes, however, remains unknown. The most thorough molecular evidence for an activator–inhibitor mechanism in animal development is from lefty-nodal signaling (30–32), which establishes a simple, binary pattern (e.g., left–right specification) and has not been shown to be involved in complex, meristic pattern formation.

Here, we provide evidence of the molecular basis of activation–inhibition mechanism underlying the formation of complex morphologies during vertebrate development. The two- and three-component activator–inhibitor models produce realistic descriptions of the interactions between Shh/Bmp2 expression and barb specification during barb ridge morphogenesis. The empirical data support the activating and inhibitory functions of Shh and Bmp2 assumed in the two-component models. The empirically supported two-component models are sufficient to describe barb morphogenesis in plumulaceous natal chick down, which lack strong D/V polarization and a rachis.

The two-component model is not sufficient to generate the more complex, D/V polarized patterns in Shh and Bmp2 signaling that are observed during barb ridge morphogenesis in pennaceous feathers (Fig. 2 *F* and *G*). But mathematical analyses further predict that Shh and Bmp2 signaling interacts with additional inhibitory and D/V polarized signal gradients in the feather germ to produce the more complicated, and evolutionarily derived, morphology of pennaceous feathers, which is characterized by ventral new barb ridge creation, helical barb ridge growth, and dorsal barb ridge fusion (Fig. 2 *I* and *J*).

The identity of a second, local (i.e., cell autonomous) Shh inhibitor has not been established experimentally, but there are several candidates supported by preliminary evidence. The Shh receptor genes Patched (Ptc) and Patched2 (Ptc2) are both transcriptionally up-regulated by Shh signaling and act as negative regulators of Shh activity (27) (see below). We know these receptors are coexpressed with Shh and Bmp2 in the epithelium of the feather (6). In addition, their cell autonomous effect on Shh signaling is precisely congruent with properties of the second inhibitor assumed in the model. However, several other members of the Shh signaling cascade involved in signal transduction (e.g., sufu) or ligand availability (e.g., Hip, Gas) may also be candidates for a Shh inhibitory function (33, 34).

Although the molecular identity of the hypothesized D/V polarized signal gradients is not established, the feather epithelium is not spatially naive. Rather, the feather germ has an inherent polarity starting from the A/P axis of the placode (D/V axis of the feather), as shown by asymmetrical expression of Shh, Bmp2, and other molecular markers in the placode epithelium (6, 12, 13). Experimental perturbations by using retinoids, thought to affect Shh signaling, can reverse orientation of the follicle such that the future dorsal ventral axis (i.e., rachis specification) is random or reversed in orientation (12). Experimental transplantations of dorsal and ventral portions of growing feather papillae demonstrate that a D/V asymmetry within the feather is involved with specifying the position of rachis formation and the direction of helical growth (35–37) as hypothesized here.

Local Activation–Inhibitor Systems as Genetic Circuits. Shh and Bmp2 do not act directly on the function of the other as idealized in the

mathematical models (available from the authors upon request). Rather, they act through signaling cascades that mediate their effects. Although we describe the expression and function of two extracellular proteins, their effect requires signaling systems containing multiple gene products for specific activator or inhibitor function. This feature promotes stable, modular function of these signaling systems, or "cassettes," that foster their evolutionary recruitment or cooption for development of novel structures in new contexts (6, 38). The integrated patterning function of Shh and Bmp2 is apparent in the formation of integumentary structures such as teeth and feathers (6, 10) and at various stages of feather growth (6). The nature of the Shh/Bmp signaling cascade would then represent a conserved epigenetic module (39) used to generate pattern and polarity during development within vertebrate integumentary appendages.

An Integrated Model of Barb Ridge Morphogenesis and Evolution. A combination of empirical and mathematical approaches supports a previously undescribed, integrated model of morphogenesis of barb ridges and the complex branched morphology of feathers.

The initial meristic patterning of the tubular feather germ epithelium into an integer number of barb ridges is accomplished by the activator–inhibitor interactions of the Shh/Bmp2 signaling module. Barb ridge growth is organized by Shh/Bmp2 signaling in the folds of marginal plate epithelium. The barb ridges themselves grow in length by the recruitment of new, naive epithelial cells that proliferate at the base of the feather germ. Shh/Bmp2 signaling organizes the recruitment of new epithelial cells to become members of a specific barb ridge. The creation of new barb ridges is accomplished by the bifurcation of the longitudinal domains, or stripes, of Shh/Bmp2 signaling in the marginal plate epithelium (6). The fusion of barb ridges occurs by the gradual reduction of the marginal plate and the loss of the distinct identity between neighboring barb ridges. Barb ridge fusion and rachis formation characteristic of pennaceous feathers occurs through gradual reduction and extinction of the epithelial signals that distinguish neighboring barb ridges on the dorsal side of the feather germ (6). In our models, the localization of barb ridge creation and fusion in pennaceous feathers is accomplished by polarized, regional modification of activator (Shh) signaling. The polarization of these processes is confirmed by the empirically demonstrated D/V asymmetry, or gradient, in the developing germs of pennaceous feathers (35–37).

A fundamental difference between the straight barb ridge growth in a simple, plumulaceous feather and the helical barb ridge growth in a pennaceous feather lies in the patterns of specification of new cells at the growing basal edges of the barb ridges. Recruitment by barb ridges of new cells from the same radial position in the feather germ as the previous cells in that ridge will produce straight barb ridge growth and a plumulaceous tuft. But recruitment of new cells from successively more dorsal positions in the feather germ will produce helical growth of barb ridges toward the dorsal side of the feather germ. Cells that originate at different times at a single position at the base of the feather germ are capable of becoming parts of the same or different barbs because of the dynamic nature of the Shh/Bmp2 signaling system that influences the development of cell identity. Our results suggest that helical growth occurs by a "traveling wave" of Shh/Bmp2 signaling that involves an additional, local Shh inhibitor in the feather epithelium (e.g., Ptc, Ptc2, Hip, or Gas).

This integrated view of barb ridge morphogenesis provides previously uncharacterized insights into the evolution of complex, pennaceous feather branching structure from more primitive plumulaceous feather structure (1, 6). The first branched feather barbs evolved through the establishment of an activator–inhibitor interaction between the plesiomorphic, or preexisting, interacting Shh and Bmp2 signaling systems in the basal epithelium (i.e., marginal plate) of the feather germ to produce meristic patterning and morphogenesis of the barbs. The subsequent plumulaceous-to-pennaceous morphological transition evolved through the derived integration of an additional short-range inhibitor and a D/V polarized signaling gradient. Thus, evolutionary novelty of pennaceous structure required the coupling of the plesiomorphic, previously independent Shh/Bmp2 module and D/V signal gradients. The signaling mechanisms that produce complex barb branching in pennaceous feathers were an inherent potential of the molecular mechanisms previously evolved with the origin of simpler, plumulaceous feathers. Integrated signaling between modular developmental systems provide both stable mechanisms of morphogenesis and inherent capacities for the generation of morphological and evolutionary novelties.

1. Prum, R. O. (1999) *J. Exp. Zool. Mol. Dev. Evol.* **285,** 291–306.
2. Prum, R. O. & Dyck, J. (2003) *J. Exp. Zool. B Mol. Dev. Evol.* **298,** 73–90.
3. Lucas, A. M. & Stettenheim, P. R. (1972) *Avian Anatomy-Integument* (U.S. Department of Agriculture Handbook, Washington, D.C.).
4. Stettenheim, P. (1976) *Proc. 16th Intl. Ornitholog. Congr.* **16,** 385–401.
5. Prum, R. O. & Williamson, S. (2001) *J. Exp. Zool. Mol. Dev. Evol.* **291,** 30–57.
6. Harris, M. K., Fallon, J. F. & Prum, R. O. (2002) *J. Exp. Zool. Mol. Dev. Evol.* **294,** 160–176.
7. Meinhardt, H. (1982) *Models of Biological Pattern Formation* (Academic, London).
8. Meinhardt, H. (1998) *The Algorithmic Beauty of Sea Shells* (Springer, Berlin).
9. Kondo, S. & Asai, R. (1995) *Nature* **376,** 765–768.
10. Salazar-Ciudad, I. & Jernvall, J. (2002) *Proc. Natl. Acad. Sci. USA* **99,** 8116–8120.
11. Gierer, A. & Meinhardt, H. (1972) *Kybernetik* **12,** 30–39.
12. Chuong, C.-M., Ting, S. A., Widelitz, R. B. & Lee, Y.-S. (1992) *Development (Cambridge, U.K.)* **115,** 839–852.
13. Widelitz, R. B., Jiang, T.-X., Chen, C. J., Stott, N. S., Jung, H.-S. & Chuong, C.-M. (1999) *Development (Cambridge, U.K.)* **126,** 2577–2587.
14. Strong, R. M. (1902) *Bull. Mus. Comp. Zool.* **40,** 147–185.
15. Cohen, J. & 'Espinasse, P. G. (1961) *J. Embryol. Exp. Morphol.* **9,** 223–251.
16. Prum, R. O. & Brush, A. H. (2002) *Q. Rev. Biol.* **77,** 261–295.
17. Meinhardt, H. & Klingler, M. (1987) *J. Theor. Biol.* **126,** 63–69.
18. Meinhardt, H. (2004) *Physica D* **199,** 264–277.
19. Meinhardt, H. (1995) *Nature* **376,** 722–723.
20. Meinhardt, H. & Gierer, A. (2000) *BioEssays* **22,** 753–760.
21. Morgan, B. A. & Fekete, D. M. (1996) in *Methods in Cell Biology*, ed. Bronner-Fraser, M. (Academic, San Diego), pp. 185–218.
22. Zho, H., Wieser, R., Massague, J. & Nisewander, L. (1997) *Genes Dev.* **11,** 2192–2203.
23. Riddle, R. D., Johnson, R. L., Laufer, E. & Tabin, C. (1993) *Cell* **75,** 1401–1416.
24. Nieto, M. A., Patel, K. & Wilkinson, D. G. (1996) in *Methods in Cell Biology*, ed. Bronner-Fraser, M. (Academic, New York), Vol. 51, pp. 219–235.
25. Morgan, B. A., Orkin, R. W., Noramly, S. & Perez, A. (1998) *Dev. Biol.* **201,** 1–12.
26. Zeng, X., Goetz, J. A., Suber, L. M., Scott, W. J., Schreiner, C. M. & Robbins, D. J. (2001) *Nature* **411,** 717–720.
27. Ingham, P. W. & McMahon, A. P. (2001) *Genes Dev.* **15,** 3059–3087.
28. Raftery, L. A. & Sutherland, D. J. (2003) *Trends Genet.* **19,** 701–708.
29. Asai, R., Taguchi, E., Kume, Y., Saito, M. & Kondo, S. (1999) *Mech. Dev.* **89,** 87–92.
30. Chen, Y. & Schier, A. F. (2002) *Curr. Biol.* **12,** 2124–2128.
31. Juan, H. & Hamada, H. (2001) *Genes Cells* **6,** 923–930.
32. Solnica-Krezel, L. (2003) *Curr. Biol.* **13,** R7–R9.
33. Jeong, J. & McMahon, A. P. (2005) *Development (Cambridge, U.K.)* **132,** 143–154.
34. Lum, L. & Beachy, P. A. (2003) *Science* **304,** 1755–1759.
35. Lillie, F. R. & Wang, H. (1941) *Physiol. Zool.* **14,** 103–133.
36. Lillie, F. R. & Wang, H. (1943) *Physiol. Zool.* **16,** 1–21.
37. Wang, H. (1943) *Physiol. Zool.* **16,** 325–356.
38. Keys, D. N., Lewis, D. L., Selegue, J. E., Pearson, B. J., Goodrich, L. V., Johnson, R. L., Gates, J., Scott, M. P. & Carroll, S. B. (1999) *Science* **283,** 532–534.
39. Von Dassow, G. & Munro, E. (1999) *J. Exp. Zool. Mol. Dev. Evol.* **285,** 307–325.